Experimental Setup Simulating Hoarfrost Formation on Roadways

Janne Siren Fjærestad[1], Johan Wåhlin[2], and Alex Klein-Paste[3]

[1]Department of Civil and Transport Engineering, Norwegian University of Science and Technology, NO-7491, Trondheim, Norway. Email: janne.fjarestad@ntnu.no

[2]Norwegian Public Roads Administration, Abels gate 5, NO-7030, Trondheim, Norway

[3]Department of Civil and Transport Engineering, Norwegian University of Science and Technology, NO-7491, Trondheim, Norway

ABSTRACT

Hoarfrost on roadways and bridges can cause slippery and dangerous conditions for motorists. To reduce the costs and environmental impacts of countermeasures the road authorities wish to optimize their winter maintenance operations. To support this, good knowledge of the hoarfrost formation process is needed. This paper presents a laboratory setup designed and built to study hoarfrost formation in detail under controlled conditions. The accumulation of hoarfrost (g/m^2) and the stability of the main controlling parameters (air temperature, surface temperature and relative humidity) are quantified. By using an open loop wind tunnel with warm, humid air flowing over a cold stone surface, we produced conditions similar to those of frost formation on a road with good stability. The hoarfrost growth rates were found to be within the range of field measurements earlier published. The growth rates were constant during each test and were directly related to the driving force created by the difference in the water vapor pressure in the air and at the stone surface.

INTRODUCTION

Hoarfrost on roadways and bridge decks can cause slippery and dangerous conditions for motorists, especially at the beginning of the winter season (Norrman et al. 2000). In Sweden in the winters of 2004-2005 and 2005-2006, 18.1% and 14.5% of accidents respectively occurred during hoarfrost formation (Andersson and Chapman 2011).

Different actions can be taken to reduce the risk of accidents due to hoarfrost, for example use of friction overlays (Evans 2010; Dave et al. 2017), monitoring road surface conditions (Minsk 1998), heating the road surface (Minsk 1999) and the application of freezing-point depressant chemicals (Ketcham et al. 1996). Due to their negative economic and environmental impacts (Ramakrishna and Viraraghavan 2005; Fay and Shi 2012) it is desirable to optimize the use of heating and chemicals. A key to this is good prediction of hoarfrost formation, both its duration and severity.

A number of models for predicting surface temperature and surface state (e.g. dry, wet, snowy, icy) on both roads and bridge decks already exist (e.g. Sass 1992; Crevier and Delage 2001; Knollhoff et al. 2003; Greenfield and Takle 2006; Denby et al. 2013 and Fujimoto et al. 2014). These models can predict when the conditions for hoarfrost formation is present. But, to the best of our knowledge, little is known about when deposited hoarfrost actually leads to slippery conditions. Since chemicals (for example sodium chloride) are frequently used during these events, it is also of interest how and how long these chemicals prevent the hoarfrost growth process. Being able to simulate hoarfrost growth in a laboratory setup will make it possible to gain further understanding of these issues when systematically adjusting the main controlling parameters of hoarfrost formation.

Several researchers have developed experimental setups for hoarfrost formation earlier. Stanton et al. (2012) used a cold ceiling to simulate long wave radiation loss due to clear sky conditions. Cheng (2003), Hermes et al. (2009) and Kandula (2011) simulated hoarfrost formation with warm humid air flowing over a cold surface. Common for these experiments is that they produced hoarfrost at much higher rates than realistic for road situations. The air temperatures were typically between 15 to 25 °C, and the frost surface temperatures were between −5 to −20 °C.

In order to study the hoarfrost formation on road surfaces in detail, we developed an experimental setup that can simulate hoarfrost formation at deposition rates that are more realistic than previous experimental setups. Similar to Cheng (2003), Hermes et al. (2009) and Kandula (2011), we extracted heat from the bottom of the surface downwards, simulating the conditions of warm humid air passing over a colder road surface. The experiment proved that this setup demonstrates sufficient stability of the key parameters and that it is possible to adjust these within a range of values relevant to winter roads.

METHOD

Theory

Hoarfrost occurs when water vapor in the air changes from a gaseous state to a solid state on a cold surface. This can occur when the surface temperature is lower than both the dew point and the temperature at which water freezes. The mechanism behind this mass transport is the difference in the energy state for water molecules in the air and at the frost surface. Water molecules will prefer the state with the lowest energy. The rate of the resulting hoarfrost growth rate can be described using different driving potentials, for example partial pressure, molar density, and mass density (Webb 1990). Using the partial pressure of water vapor as the driving potential, the rate of the resulting frost growth can be described as:

$$\dot{m} = K_p(p_{v,a} - p_{v,fs}) \tag{1}$$

where K_p is the mass transfer coefficient, $p_{v,a}$ is the water vapor pressure in the air flow and $p_{v,fs}$ is the water vapor pressure at the frost surface.

The water vapor pressure in the air, $p_{v,a}$, is calculated from the definition of the relative humidity:

$$RH = \frac{p_{v,a}}{p_{v,a}^{sat}} \cdot 100 \tag{2}$$

where RH is the measured relative humidity and $p_{v,a}^{sat}$ is saturation vapor pressure at the given air temperature, T_a.

Air is assumed to be saturated at the frost surface (Kandula 2011). The water vapor pressure at the frost surface, $p_{v,fs}$, is therefore given as the saturation vapor pressure at the surface temperature, T_s.

Hoarfrost growth

A setup as shown in Fig. 1 was build inside a walk-in cold temperature laboratory. The setup was designed to simulate typical conditions for frost formation on road surfaces, with air velocities ranging from 0.6 m/s to 1.2 m/s, relative humidity from 60% to 100%, air temperatures from −20 °C to 5 °C, and surface temperatures ranging from air temperature to 8 °C below air temperature.

The setup was designed as an open loop wind tunnel in which humid air flowed over a cold stone surface, see sketch in Fig. 2. The air flow was driven by tangential fan 1 placed at the end of the loop. The wind speed, v, was measured at a location 1.5 cm above the stone surface using a Fluke 975V AirMeter (sensor 3) and controlled by adjusting the fan voltage. Water vapor was added to the air by placing a water bath in front of the stone surface. The amount of vapor added could be controlled by adjusting the water temperature and the open area of the water bath, using an adjustable lid. During tests it was found to be easier to adjust the lid than the bath temperature. A bath temperature of 25 °C was used for the tests presented here. The build-up of hoarfrost took place on an 80 mm x 80 mm stone with a height of 9 mm. Typical asphalt concrete consists of 95% stone and 5% mastic, which is bitumen and filler. Therefore, it was decided to use a stone in order to achieve an even heat transfer through the test sample and to avoid potential artifacts due to the presence of mastic. The stone was cooled by 4 Peltier elements connected in series. The cooling of the Peltier elements took place in a separate wind loop below the humidity transport loop. The two loops were separated by a 5 cm thick layer of XPS insulation placed around the stone. The Peltier elements were placed on a pin fin heat sink, and an additional fan (fan 2 in Fig. 2) was added below the insulation to improve the heat convection from the warm side of the Peltier elements. The stone surface temperature was controlled by adjusting the voltage on the Peltier elements.

The different parameters measured during the experiments are listed in Table 1. The real-time amount of hoarfrost deposited on the stone surface, m_r, was logged using an electronic scale during frost formation. To control this real time measurement of the mass, the stone was also removed from the setup and weighed on another electronic scale before and after each frost growth test. This manually measured mass difference between the start and end of each test was denoted m_m.

The relative humidity, RH, was measured using a Vaisala HMT337 sensor with a warmed probe allowing measurements up to 100% RH. The humidity sensor was calibrated at 2 °C by an HMK15 calibration kit, using NaCl as reference.

The air temperature inside the setup, T_a, was measured with a temperature probe integrated in the Vaisala HMT337 sensor. Humidity and air temperature were measured 9 cm in front of the stone at a height of 2.5 cm above the stone surface (sensor 1 in Fig. 2). The surface temperature of the stone, T_s, was measured using a Pt100 glued at a corner of the stone (sensor 2). The temperature sensors were calibrated in a slush of finely crushed ice and water.

RESULTS

In total 15 frost growth tests were performed. Ten were performed with an air temperature of 2 °C, and five with an air temperature set to −15 °C. These two test series are referred to as performed at $T_a = 2$ °C and $T_a = -15$ °C, even though the measured T_a varied between the different tests. Wind speed was held constant at 0.6 m/s for all tests. The difference in the water vapor pressure in the air and at the stone surface was varied by adjusting the temperature of the stone surface and the relative humidity in the air. The average relative humidity ranged between 58.9% and 91.4% across the different tests, and the maximum obtained difference between air temperature and stone surface temperature was 8.5 °C.

An overview of the measured and calculated parameters and their standard deviations, is found in Table 2. Data were sampled at a frequency of 2.4 Hz and filtered over 1000 measurements, i.e. 6.9 minutes, using a rolling mean filter. Analysis was performed from the point when the surface temperature dropped below the dew point. The stability of the different parameters and the mass accumulation during a typical frost growth test are shown in Fig. 3. In the test shown i Fig. 3 the average relative humidity was 59.9%, with a maximum value of 61.3% and a minimum value of 58.9%. The average air temperature was 0.7 °C, fluctuating between 0.6 °C and 0.8 °C. The temperature of the stone decreased in the first minutes of the test before it stabilized at −7.8 °C.

The real time measured mass, m_r, showed small deviations over time compared to the manually measured mass, m_m, found by weighing the stone before and after frost growth. This is likely to be due to the scale drifting. All hoarfrost growth rates are therefore calculated based on the manually measured mass, m_m.

Fig. 4 shows (a) the stone without hoarfrost, (b) typical frost growth after tests performed at $T_a = 2\,°C$ and (c) at $T_a = -15\,°C$. The frost pattern is homogenous in both images, indicating that the surface temperature of the stone is homogeneous. At 2 °C the frost structure is dense, while at −15 °C there is a coarser frost structure with more air between each crystal.

Fig. 5 shows the frost growth rate, $\dot{m}$, as a function of the difference in the vapor pressure in the air and at the frost surface for all tests. The frost growth rate was found as the measured mass, m_m, divided by the stone area and the time used for each test. $p_{v,a}$ was calculated from the measured mean values of RH and T_a and $p_{v,fs}$ was calculated from the measured mean value of T_s. Tests with air temperature $T_a = 2\,°C$ are marked with crosses and those with $T_a = -15\,°C$ are marked with dots. A linear trend is shown and there are no distinct differences between the results from the two different air temperatures. Linear regression was used to find the mass transfer coefficient, K_p, in Eq. (1). $K_p = 1.35 \times 10^{-7}\,\mathrm{kg\,m^{-2}\,s^{-1}\,Pa^{-1}}$ is valid for the setup with a wind speed of 0.6 m/s. Data from both temperatures were used, and the coefficient of determination, R^2, was found to be 0.99. The linear regression was forced through the origin to ensure zero hoarfrost growth when the partial vapor pressure difference was zero.

DISCUSSION

The total amount of hoarfrost formed in the tests ranged from 125 to 750 $\mathrm{g/m^2}$ with rates ranging from 16 to 84 $\mathrm{g/m^2h}$. Karlsson (2001) reports amounts of hoarfrost deposited during one night in the range of 55 to 495 $\mathrm{g/m^2}$. The rates are not given, but by assuming 12 h of frost growth during each test it can be estimated that they are in the range of 5 to 41 $\mathrm{g/m^2h}$. If any sublimation occurred during this period, the real rates are higher. Both the total amount of hoarfrost and the rates from the laboratory setup are thus realistic.

The stability of the key parameters such as air temperature, surface temperature and humidity is seen as sufficient for the purpose during the tests. As shown in Fig. 3 (d) a constant frost growth rate was seen during the entire frost growth period in our test. The same linear growth was seen in all tests. The water vapor pressure in the air ($p_{v,a}$) was held constant during the tests. The constant frost growth rate ($\dot{m}$) implies that the vapor pressure at the frost surface also remained constant. This can only be the case if the frost surface temperature remained reasonably constant, while the frost layer grows. This was confirmed by temperature measurements with an IR thermometer revealing a temperature stability on the top surface of the frost within ±0.5 °C during a typical frost growth period. It can therefore be argued that the cooling of the frost surface is not limited by the transport of heat through the frost layer for the amounts of hoarfrost ($125 - 750\text{g/m}^2$) and the temperature conditions ($T_a - T_s < 9\,°\text{C}$) studied here. Despite the constant growth rate in all the test runs, the deviation between m_r and m_m varied between the different tests. This variation did not correlate with the difference in the temperature or the duration of the tests. We believe the key problem is related sensor drift, as the sensor can only be reset to zero at the beginning of the test. This problem could be solved by building an automated system for lifting the stone from the scale during the tests, making it possible to perform a consecutive series of weight measurements with the scale tared before each measurement. It would also be possible to determine the mass development of the hoarfrost throughout the tests by performing manual weight measurements at specific time intervals.

The ability to produce and measure realistic amounts of hoarfrost under realistic road surface conditions is valuable for further understanding the following issues:

- how different amounts or types of hoarfrost affects the road surface friction
- how the hoarfrost formation process is influenced by the presence of salt
- the dilution rate of applied anti-icing agents

All these phenomena are important when optimizing the use of measures to avoid slippery roads due to hoarfrost formation, for both deciding when to use them and for estimating their duration.

CONCLUSION

A setup specifically made to study hoarfrost under conditions relevant to winter road maintenance was designed and built. By using an open loop wind tunnel with warm, humid air flowing over a cold stone surface we were able to produce conditions similar to those of frost formation on a road with good stability. The hoarfrost growth rates were found to be within the range of field measurements earlier published. This makes the setup suitable for studying issues related to hoarfrost formation on roads such as friction and salting dosage.

The hoarfrost growth rate was found to be constant during the frost growth tests, irrespective of the thickness of the hoarfrost layer. This indicates that the frost surface temperature was stable throughout each test for the amounts of frost ($125 - 750\mathrm{g/m^2}$) and temperatures ($T_a - T_s < 9\,°\mathrm{C}$) studied here.

DATA AVAILABILITY STATEMENT

Data generated in the laboratory experiment and calculated data used in presented figures are available from the corresponding author by request.

ACKNOWLEDGEMENTS

This study is sponsored by the Norwegian Public Roads Administration (NPRA) as part of the research program initiated by NPRA associated with the E39 coastal highway route along the west coast of Norway.

The authors would like to thank Bent Lervik, Per Asbjørn Østensen, Frank Stæhli and Tage Wessum for their technical support during the design and construction of the experimental setup.

REFERENCES

Andersson, A. and Chapman, L. (2011). “The use of a temporal analogue to predict future traffic accidents and winter road conditions in Sweden.” *Meteorological Applications*, 18(2), 125–136.

Cheng, Chin-Hsiang; Wu, K.-H. (2003). “Observations of early-stage frost formation on a cold plate in atmospheric air flow.” *Journal of Heat Transfer*, 125, 95–102.

Crevier, L.-P. and Delage, Y. (2001). “Metro: A new model for road-condition forecasting in Canada.” *Journal of Applied Meteorology*, 40(11), 2026–2037.

Dave, E. V., Kostick, R. D., and Dailey, J. (2017). “Performance of high friction bridge deck overlays in crash reduction.” *Journal of Performance of Constructed Facilities*, 31(2), 04016094.

Denby, B. R., Sundvor, I., Johansson, C., Pirjola, L., Ketzel, M., Norman, M., Kupiainen, K., Gustafsson, M., Blomqvist, G., Kauhaniemi, M., and Omstedt, G. (2013). "A coupled road dust and surface moisture model to predict non-exhaust road traffic induced particle emissions (NORTRIP). Part 2: Surface moisture and salt impact modelling." *Atmospheric Environment*, 81, 485–503.

Evans, J. F. (2010). "Evaluation of the SafeLane™ overlay system for crash reduction on bridge deck surfaces." *Report No. MN/RC 2010-13*, Minnesota Department of Transportation Research Services Section.

Fay, L. and Shi, X. (2012). "Environmental impacts of chemicals for snow and ice control: State of the knowledge." *Water, Air, & Soil Pollution*, 223(5), 2751–2770.

Fujimoto, A., Tokunaga, R., Kiriishi, M., Kawabata, Y., Takahashi, N., Ishida, T., and Fukuhara, T. (2014). "A road surface freezing model using heat, water and salt balance and its validation by field experiments." *Cold Regions Science and Technology*, 106–107, 1–10.

Greenfield, T. M. and Takle, E. S. (2006). "Bridge frost prediction by heat and mass transfer methods." *Journal of Applied Meteorology and Climatology*, 45(3), 517–525.

Hermes, C. J., Piucco, R. O., Barbosa Jr., J. R., and Melo, C. (2009). "A study of frost growth and densification on flat surfaces." *Experimental Thermal and Fluid Science*, 33(2), 371–379.

Kandula, M. (2011). "Frost growth and densification in laminar flow over flat surfaces." *International Journal of Heat and Mass Transfer*, 54(15–16), 3719–3731.

Karlsson, M. (2001). "Prediction of hoar-frost by use of a road weather information system." *Meteorological Applications*, 8(01), 95–105.

Ketcham, S. A., Minsk, L. D., Blackburn, R. R., and Fleege, E. J. (1996). "Manual of practice for an effective anti-icing program: A guide for highway winter maintenance personnel." *Report No. 2/22/96*, US Army Cold Regions Research and Engineering Laboratory.

Knollhoff, D. S., Takle, E., Gallus, W., Burkheimer, D., and McCauley, D. (2003). "Evaluation of a frost accumulation model." *Meteorological Applications*, 10(4), 337–343.

Minsk, L. D. (1998). *Snow and Ice Control Manual for Transportation Facilities*. McGraw-Hill.

Minsk, L. D. (1999). “Heated bridge technology.” *Report No. FHWA-RD-99-158*, U.S Department of Transportation, Federal Highway Administration.

Norrman, J., Eriksson, M., and Lindqvist, S. (2000). “Relationships between road slipperiness, traffic accident risk and winter road maintenance activity.” *Climate Research*, 15, 185–193.

Ramakrishna, D. M. and Viraraghavan, T. (2005). “Environmental impact of chemical deicers – A review.” *Water, Air, and Soil Pollution*, 166(1), 49–63.

Sass, B. H. (1992). “A numerical model for prediction of road temperature and ice.” *Journal of Applied Meteorology*, 31(12), 1499–1506.

Stanton, B., Miller, D., and Adams, E. (2012). “Analysis of surface hoar growth under simulated meteorological conditions.” *Proceedings, 2012 International Snow Science Workshop, Anchorage, Alaska*.

Webb, R. L. (1990). “Standard nomenclature for mass transfer processes.” *International Communications in Heat and Mass Transfer*, 17(5), 529–535.

List of Tables

TABLE 1. Overview of measured parameters

Parameter	Symbol	Unit	Instrument
Humidity	RH	%	Vaisala HMT337
Air temperature	T_a	°C	Vaisala HMT337
Surface temperature	T_s	°C	Pt100
Air velocity	v	m/s	FLUKE 975V
Mass of hoarfrost from real time measurements	m_r	g	OHAUS Pioneer PA2202
Mass of hoarfrost from manual measurement	m_m	g	AND EK-400H

TABLE 2. Overview of measured and calculated parameters from all tests

Test #	Test duration (h)	Accumulated hoar frost (g/m^2)	Frost growth rate (g/m^{2}h)	Average relative humidity RH (%)	Average air temperature T_a (°C)	Average stone surface temperature T_s (°C)	Average dew point temperature T_d (°C)
1	1.7	141	84	77.9 ± 3.2	1.2 ± 0.3	−6.0 ± 0.3	−2.3 ± 0.8
2	2.7	219	81	86.8 ± 1.3	2.1 ± 0.1	−3.6 ± 0.1	0.1 ± 0.2
3	3.1	125	40	88.2 ± 3.5	2.0 ± 0.3	−1.4 ± 0.2	0.3 ± 0.8
4	2.8	187	68	78.3 ± 1.9	2.0 ± 0.1	−4.5 ± 0.1	−1.4 ± 0.3
5	3.8	188	50	71.1 ± 1.6	1.2 ± 0.2	−5.9 ± 0.2	−3.4 ± 0.4
6	3.2	234	74	75.8 ± 1.5	1.9 ± 0.1	−6.2 ± 0.1	−1.9 ± 0.3
7	4.6	141	31	59.9 ± 0.5	0.7 ± 0.0	−7.8 ± 0.0	−6.2 ± 0.1
8	18.8	297	16	58.9 ± 0.6	0.6 ± 0.1	−6.6 ± 0.1	−6.5 ± 0.1
9	23.6	750	32	62.9 ± 1.4	0.6 ± 0.1	−7.5 ± 0.1	−5.6 ± 0.3
10	22.3	453	20	64.5 ± 1.3	0.7 ± 0.0	−5.9 ± 0.0	−5.3 ± 0.3
11	18.7	438	23	74.2 ± 3.7	−16.4 ± 0.3	−24.2 ± 0.3	−20.0 ± 0.9
12	42.9	672	16	74.1 ± 3.2	−16.5 ± 0.3	−22.0 ± 0.3	−20.0 ± 0.8
13	21.5	375	17	73.7 ± 3.4	−16.6 ± 0.3	−22.3 ± 0.3	−20.1 ± 0.8
14	5.8	234	41	82.0 ± 1.0	−13.9 ± 0.3	−21.5 ± 0.2	−16.3 ± 0.2
15	4.0	204	51	91.4 ± 2.7	−13.5 ± 0.4	−21.3 ± 0.2	−14.7 ± 0.5

List of Figures

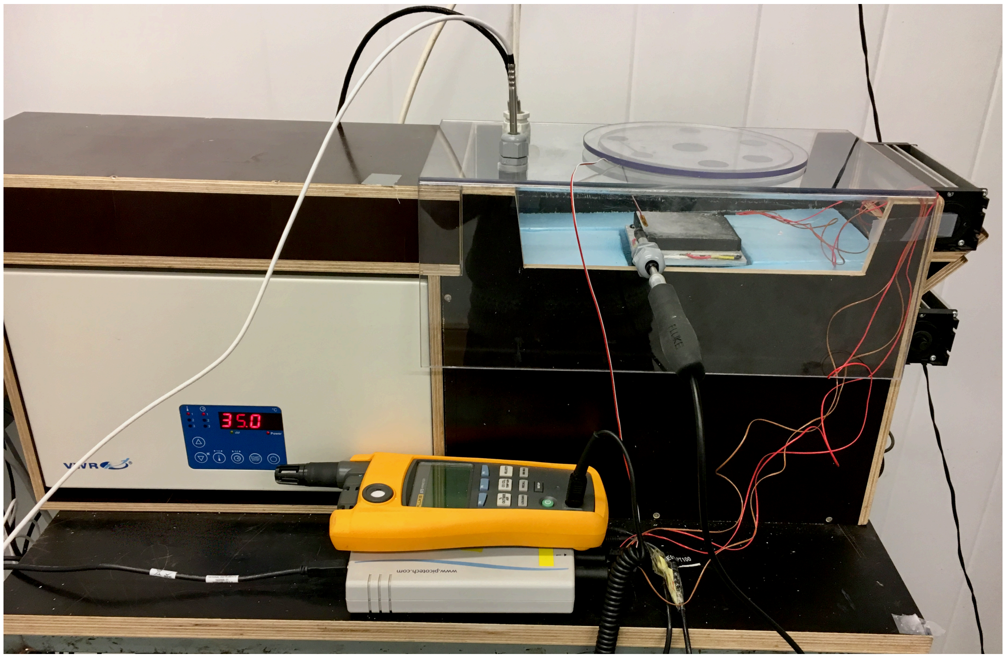

Fig. 1. Picture of experimental setup

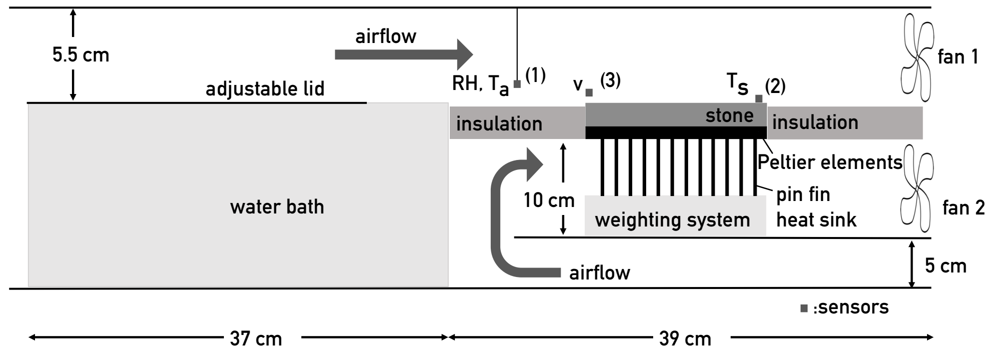

Fig. 2. Sketch of experimental setup showing how humid air flows over the cold stone surface resulting in hoarfrost formation. Sensor 1 measures RH and T_a and is located 9 cm in front of the stone at a height of 2.5 cm above the stone surface. Sensor 2 measures T_s and is located at the corner of the stone. Sensor 3 measures wind speed and is located in front of the stone at a height of 1.5 cm.

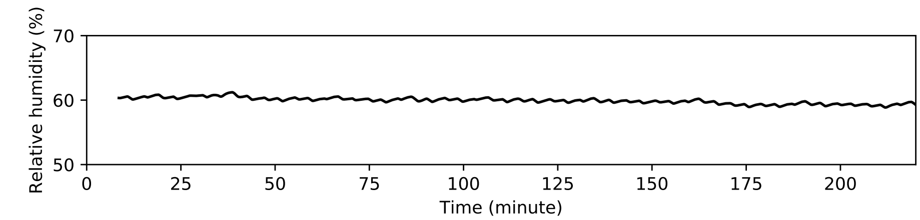

(a)

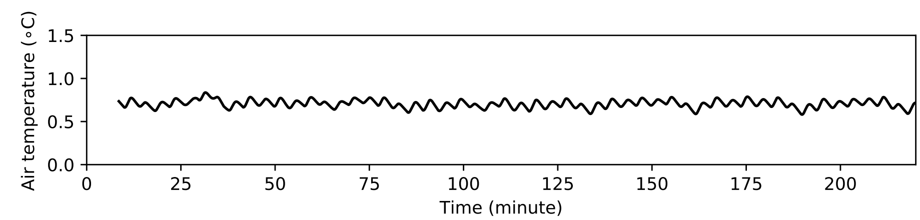

(b)

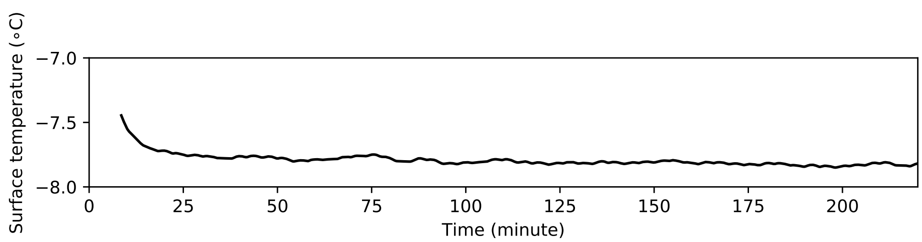

(c)

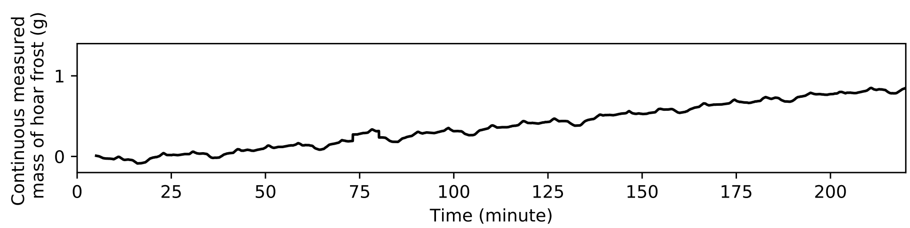

(d)

Fig. 3. Stability of measured parameters during test 7: (a) relative humidity, (b) air temperature, (c) surface temperature, (d) real time measured mass of hoarfrost, m_r.

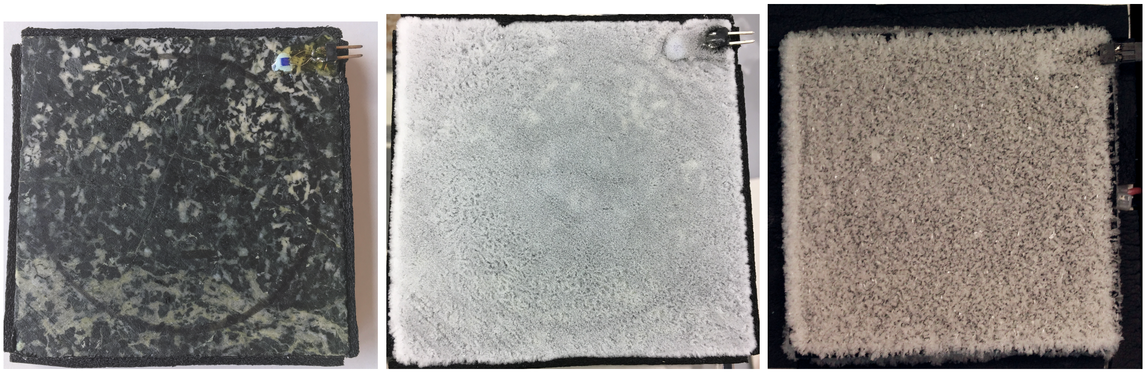

(a) **(b)** **(c)**

Fig. 4. Image of (a) stone without hoarfrost, (b) frost growth at the end of test number 4, (c) frost growth at the end of test number 12.

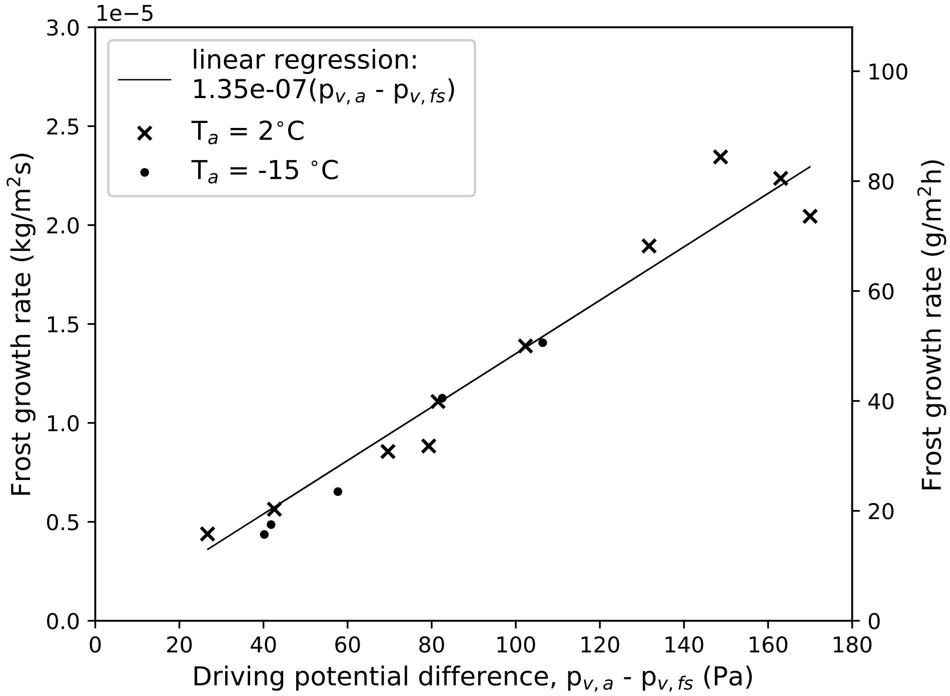

Fig. 5. Frost growth rate as a function of the difference in the vapor pressure in the air and at the frost surface.